Stress Paths on Displacement Piles During Monotonic and Cyclic Penetration

Jakob Vogelsang(✉), Gerhard Huber, and Theodoros Triantafyllidis

Institute of Soil Mechanics and Rock Mechanics,
Karlsruhe Institute of Technology, Karlsruhe, Germany
jakob.vogelsang@kit.edu

Abstract. In this contribution, a study on the behavior of instrumented model piles in slow, cyclic penetration tests using a cylindrical full model test set-up is presented. The tests are performed under 1g-conditions in a uniform medium sand. A hydraulic driving system enables a displacement controlled penetration similar to the pile motion during vibro-driving at strongly reduced frequency. The pile instrumentation allows the measurement of shaft and tip force during the driving process. Systematic variation of soil density and displacement amplitude reveals the occurrence of typical stress paths of vibratory pile penetration. By comparison with results from monotonic and vibratory penetration tests, the influence of the penetration mode is deduced. Results from FE simulations applying a hypoplastic soil model help to illustrate the strong requirements and the considerable challenges to obtain realistic simulations of cyclic pile penetration processes. Some hints towards a further numerical modeling of the tests are given.

Keywords: Displacement pile · Monotonic penetration · Cyclic penetration · Vibratory pile driving

1 Vibratory and Cyclic Pile Penetration

Vibratory pile driving bases on the application of a harmonic excitation to a vibrator-pile system in order to facilitate the penetration compared to jacking or impact driving. The pile motion during vibro-penetration is a result of the excitation, the dynamic properties of the pile-vibrator system and the soil response. In practice, the range of applied frequencies is 15 to 50 Hz and typical displacement amplitudes lie within 5–15 mm resulting in penetrations per cycle of vibration of about 1–10 mm [4,15]. Generally speaking, dense cohesionless soils require high displacement amplitudes whereas in loose soil, it is helpful to use high frequencies [15].

The global penetration behavior and the evolution of tip resistance depend qualitatively on the combination of displacement amplitude and penetration per cycle of vibration. However, in cohesionless soils and in the scope of application, the tip resistance is independent of the current penetration velocity. High penetration rates, the so-called fast vibratory driving, is characterized by the reach

T. Triantafyllidis (ed.), *Holistic Simulation of Geotechnical Installation Processes*,
Lecture Notes in Applied and Computational Mechanics 82, DOI 10.1007/978-3-319-52590-7_2

of a limit tip resistance comparable to monotonic penetration resistance. The beneficial effect of eased penetration is obtained for larger ratios of amplitude and penetration per cycle, the so-called slow vibratory pile driving [4,15]. These dependencies are qualitatively well known, although there is still a considerable lack of understanding the soil mechanical processes and of concise prognosis tools for the driving process. Although FE simulations have been shown to be able to qualitatively reproduce the major effects, their systematic and quantitative validation is still under research.

The shaft friction in a given depth depends on the radial stress acting on the pile shaft and the friction coefficient between soil and shaft. It is also independent of shearing velocity for cohesionless soils. While the friction coefficient can be estimated or measured with sufficient accuracy, knowledge about the radial stress distribution is difficult to be obtained. Although it is reasonable to assume a qualitatively increasing stress with depth, simple estimations e.g. done by Dierssen [5] fail to explain the observed mechanisms, notably, the so-called friction fatigue effect: the decreasing radial stress in a given depth with increasing pile penetration [9,11,20]. This degradation of stress along the pile shaft is a function of depth, soil density, number and amplitude of cycles and pile diameter [11,14,20]. The quantitative incorporation of all these effects in numerical simulations is currently not possible.

Laboratory model tests on pile penetration are useful to gain a better understanding of the process and to obtain experimental data for comparison with numerical simulations. However, dealing with vibratory pile penetration, the test results may be influenced by boundary effects and the tests therefore be problematic for numerical simulations. Accounting for the velocity-independence of the soil resistance during vibro-penetration, cyclic penetration tests at strongly reduced frequency are frequently used to overcome some of these limitations and to incorporate major effects of vibratory penetration at the same time [8,11,20]. The cyclic pile motion is now imposed. It can thus be maintained constant throughout a test and is easily varied from test to test. Although e.g. White and Lehane [20] highlight the role of cyclic pile motion, it is interesting to note that a systematic investigation of its influences has not been carried out until now.

The present study tries to contribute to this research in order to close the knowledge gap and to provide valuable experimental data for comparison with numerical simulations. The objective is to investigate whether slow cyclic penetration tests can be used to observe effects similar to vibratory pile driving and to perform a parametric study on the influence of soil density, pile displacement amplitude and penetration depth. The cyclic penetration tests are interpreted with respect to monotonic penetration tests for three different initial densities. A systematic investigation of the process is achieved by application of prescribed cyclic displacement sequences maintained throughout each test. Due to the concentration on slow tests, a wide range of numerical models should be applicable for the simulation of the tests. Some numerical back-calculations of the tests are also given in this paper.

2 Experimental Setup

2.1 Experimental Setup

The basic test setup is schematically illustrated in Fig. 1(a). It is also described in detail in [19]. The model tests are performed in a cylindrical test container of stainless steel. The container has an inner diameter of 0.94 m and a height of 1.45 m measured from the bottom of the container. It is filled with dry sand, thus, the inner dimensions of the test container correspond to the initial sample geometry. An instrumented model pile is penetrated into the sand by means of an actuator unit mounted on top of the container. The actuator unit consists of a loading frame installed with a differential hydraulic actuator allowing a maximum stroke of about 1.2 m. Typical penetration depths reached in the tests are about 1 m. The actuator is operated by a hydraulic aggregate and is equipped with a control valve allowing the application of two-way displacement sequences.

The model pile has a diameter of 50 mm and about 1.4 m length. It is manufactured of a stainless steel tube with 2 mm thickness and has an instrumented pile tip. The tip has an angle of aperture of 60°. The friction angle between pile surface and test sand can be estimated to $12 \div 15°$ based of the results of interface tests [19]. Above the pile head, a 0.46 m long spacer is placed to take advantage of the full cylinder stroke for pile penetration. The spacer is connected to the hydraulic piston.

The ratio of test container and pile diameter is rather small ($d_C/d_{pile} \approx 19$) and the container wall can be considered as rigid. Thus, significant boundary effects are expected in the experiments leading to an increase of penetration resistance compared to free-field conditions, particularly in dense sand [4,19]. However, the tests are comparable between each other and the lateral boundary conditions can be implemented in a numerical model so that the basic requirements for benchmark experiments are fulfilled.

Two types of tests can be performed with the current setup: monotonic and cyclic penetration tests. In monotonic tests, the pile penetration is conducted with a constant velocity of 3 mm/s. Cyclic tests consist of alternating phases of downward motion with approximately 3 mm/s and upward motion with about 5 mm/s. The control valve for the hydraulic actuator is therefore connected to the data acquisition. In the case of cyclic tests, the measurement of pile displacement is sampled and the valve is switched according to the desired sequence of downward and upward pile motion. The amount of downward and upward motion can be prescribed with sufficient accuracy after some calibration procedures. The frequency is in the range of $0.25 \div 1$ Hz leading to moderate accelerations at the pile toe of about 0.2 g max. around the reversal phases of pile motion.

2.2 Instrumentation

At the pile head, the displacement and the head force are measured. A potentiometric cable transducer which is attached to the connection cross bar measures the relative displacement between pile head and loading frame. The load cell for

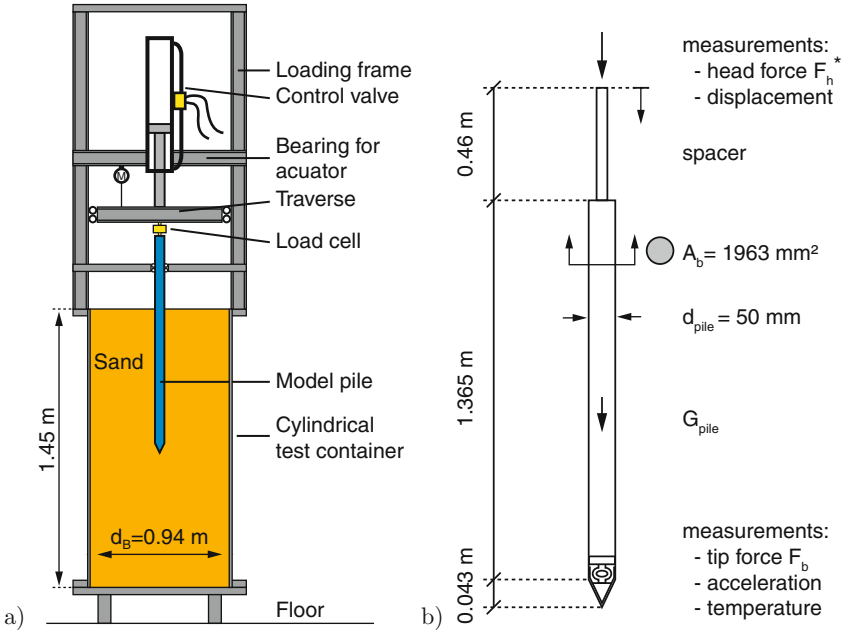

Fig. 1. (a) Basic test setup for the model tests and (b) measurements on the instrumented model pile

the pile head force is self-fabricated and connects the pile head to the traverse. It has a measuring range of 50 kN, a resolution of 0.01 kN and a linearity error smaller than 0.5%.

The pile tip is instrumented with a load cell, an acceleration transducer and a temperature measurement. The load cell (in-house manufacture) is designed for 10 kN maximum load with 0.5% linearity error, Fig. 2. Detailed information about the design and the characteristics of the load cell can be found in [19]. For acceleration, an ICP-transducer and for temperature, a micro PT-100-type sensor are used.

The measurements are recorded using a multichannel system with simultaneous sampling and digital filtering (16 bit, 400 Hz sampling rate and 40 Hz Bessel lowpass filter, 4th order).

Figure 1(b) shows the nomenclature for the measured values that are used for the interpretation in this paper. $u_{y,pile}$ indicates the position of the pile shoulder relative to the initial level of the sand surface, resp. the upper edge of the test container. The overall penetration resistance is named F_h and corresponds to the measured head force F_h^* subtracted by the pile weight G_{pile}. The tip resistance is expressed in terms of the measured tip force F_b and the tip pressure $q_b = F_b/A_b$. The shaft friction force can be calculated as the difference between overall and tip resistance, $F_s = F_h - F_b$.

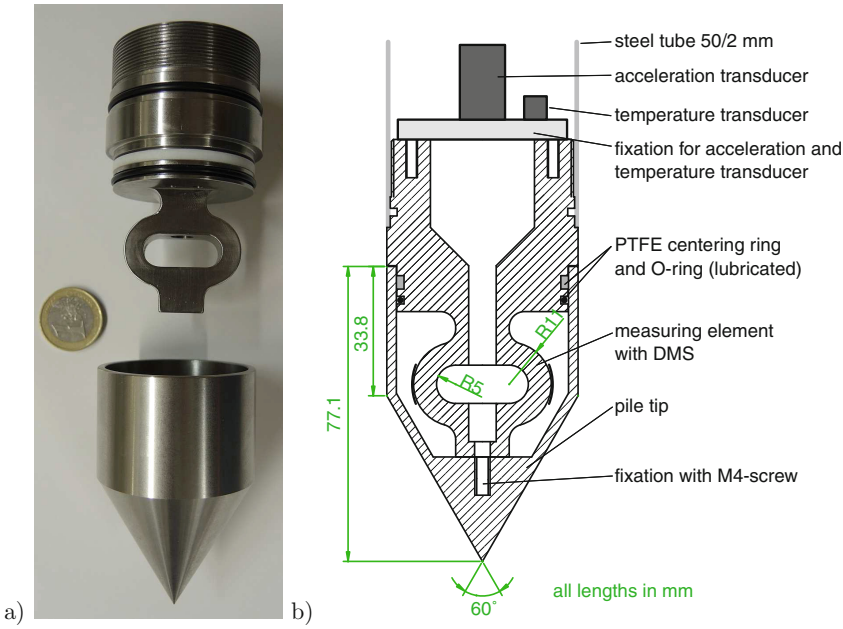

Fig. 2. Self-fabricated instrumented model pile tip: (a) Photo and (b) cross section

2.3 Test Sand and Sample Preparation

A uniform medium quartz sand is used in the present study. The minimum and maximum void ratios are $e_{min} = 0.557$ and $e_{max} = 0.873$. Compared to other studies of the authors [18,19], the test sand has slightly more fine content and different index void ratios, however, it remains very similar. Figure 3 shows a typical grain size distribution determined for the sand of the present series (2016) in comparison with sand of an older charge (2013).

A rainer system is used to pluviate the dry sand into the test container. Different initial densities are achieved by variation of the free fall height and pluviation intensity. Loose samples are prepared using a rigid tube and zero free fall height by building up a soil cone, according to the ASTM Standard [1] or DIN 18126 [6] procedures. As can be seen in Table 1, the achieved relative densities actually are about zero, which proves that the method also works in a larger scale. Medium dense and dense samples are built up in horizontal layers using a diffusor with 0.15 to 0.3 m free fall height and low intensity. High free fall heights and low intensities lead to higher densities [3,19]. A detailed description of the preparation and uniformity control methods is provided by Vogelsang [19].

2.4 Experimental Program

The test series discussed here comprises 9 penetration tests including 3 monotonic (MON) and 6 cyclic tests (CYC). Three different initial densities

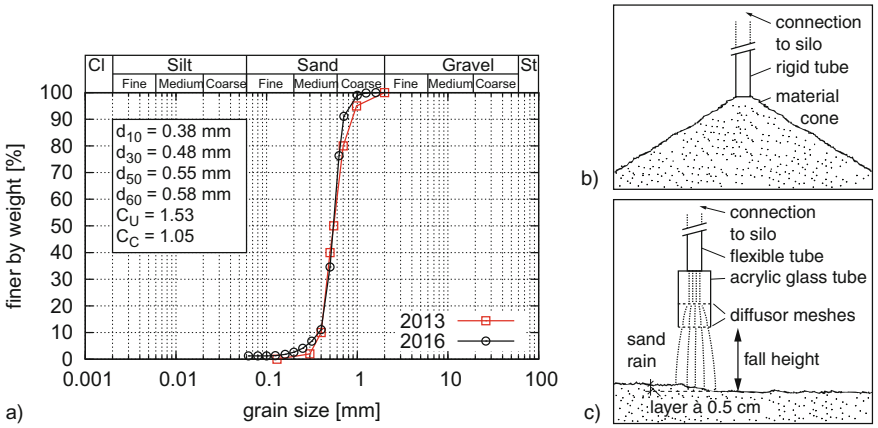

Fig. 3. (a) Grain size distributions of the test sand in comparison with sand from previous studies, (b) sand deposition procedure for loose samples and (c) for medium dense and dense samples.

have been investigated: loose, medium dense and dense. For each density a set consisting of a monotonic test, a cyclic test with small amplitude and a cyclic test with large amplitude has been performed. Information concerning the initial conditions and the performed test paths are given in Table 1.

The designation of the tests follows [19], where also additional test results can be found. The value y_0 corresponds to the initial vertical height of the pile shoulder above the sand surface (Fig. 4 - test start) and in the column $u_{y,pile}$, the test path is characterized. In the case of monotonic penetration, only the maximum penetration depth is given (relative to the pile shoulder). For cyclic tests, the values in brackets describe the performed sequence of downward and upward motion. For the discussion of the test results the variable $u_{y,pile}$ is used

Table 1. Test information for the present study

Test	Date	e_0 [−]	$I_{D,0}$ [−]	Type	y_0 [mm]	$u_{y,pile}$ [mm]
VM-06	15.02.16	0.8655	0.024	MON	35	−1050
VM-07	17.02.16	0.8746	−0.005	CYC	35	−1030 (−10/+4)
VM-10	18.03.16	0.6958	0.561	CYC	67	−1010 (−10/+4)
VM-11	07.04.16	0.6990	0.551	MON	67	−1010
VM-12	13.04.16	0.7019	0.542	CYC	66	−1080 (−5/+1)
VM-15	24.05.16	0.6001	0.864	CYC	69	−635 (−10.3/+4.3)
VM-16	17.06.16	0.6001	0.864	MON	73	−660
VM-17	06.07.16	0.5990	0.867	CYC	74	−630 (−6.9/+3)
VM-20	19.10.16	0.8707	0.007	CYC	74	−1080 (−5/+1)

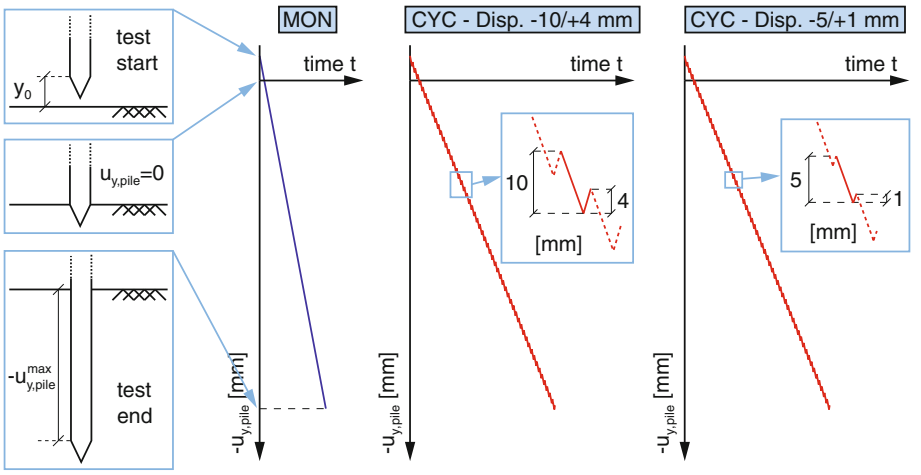

Fig. 4. Schematic illustration of the test paths performed for the present study

indicating the current vertical position of the pile shoulder below the sand surface (negative values for positions below the sand surface).

In the first group of tests, alternations of a penetrative motion of ca. 10 mm and upward motions of about 4 mm are conducted. This displacement sequence will be characterized as cyclic displacement with large amplitude. The other cyclic test path corresponds to penetration phases of about 5 mm and pullout phases of approximately 1 mm. These tests will be named tests with small displacement amplitude. The test paths are schematically illustrated in Fig. 4.

3 Test Results

3.1 Global Penetration Resistance

The first results in Fig. 5 are illustrating the evolution of penetration resistance in monotonic tests. The curves of the three tests will be displayed in the subsequent figures and serve as a reference for the cyclic tests.

It can be seen that the magnitude of penetration resistance changes depending on the initial soil density. The resistance in medium dense sand is about 10 times and in dense sand about 20 times larger than in loose sand. Therefore, in the subsequent figures, individual scales will be used for the different densities.

Apart from the magnitude of measured force, the qualitative shape of the evolution of penetration resistance is density-dependent. According to the description of penetration resistance in sand given by Linder [12], the penetration process can be divided in three important phases. The first phase of penetration resembling to the behavior of shallow foundations cannot be distinguished, probably to the conical pile tip. The two other important phases of penetration can be observed for the tests in loose and medium dense sand: a transition phase

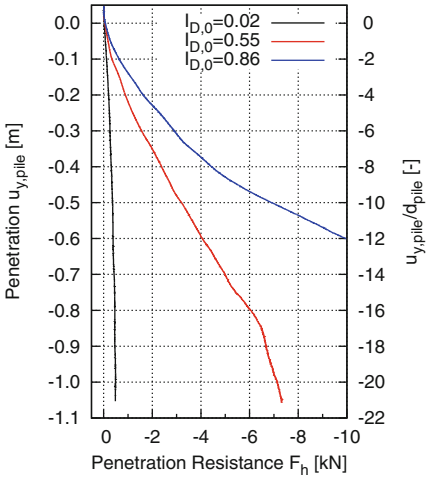

Fig. 5. Comparison of the penetration resistance in monotonic tests

with very slowly increasing resistance and a phase of quasi-constant penetration resistance (Linder [12]). Especially in medium dense sand, the reaching of the third phase of quasi-constant resistance is very marked in a depth of about $16d_{\text{pile}}$. In loose sand, the phase of constant resistance is also very pronounced (better to see in Fig. 6). On the other hand, in dense sand, the transition to the third phase is not reached. The rapidly increasing resistance in dense sand is indicating a strong jamming effect related to the low ratio of container/pile diameter.

Figure 6 shows a comparison of the penetration resistance in cyclic and monotonic penetration tests of the present series. The upper row corresponds to the tests with large amplitude ($\approx -10/+4$ mm) and the lower row to the tests with smaller amplitude ($\approx -5/+1$ mm). The left hand side shows the results in loose sand, the middle those in medium dense and the right hand side the tests in dense sand. This composition is maintained throughout the subsequent figures. The tests in dense sand were only performed to a depth of about 0.65 m because the maximum force of the tip load cell was reached.

Figure 6 shows an alternation of large compressive forces in the penetration phases and slightly positive forces during upward motion. The penetration resistance is composed of tip and shaft force, whereas the pullout force is attributed only to the shaft force. The interpretation of the results is first done based on the envelope curves, in other words the maximum penetration and pullout resistance. Afterwards, the behavior during individual cycles will be considered in detail.

The maximum penetration force in a given depth is clearly related to the monotonic penetration resistance. Thus, the envelope of the penetration force has a similar shape as the monotonic curve. In loose sand, the monotonic resistance is slightly exceeded, probably due to a stronger densification of the material around

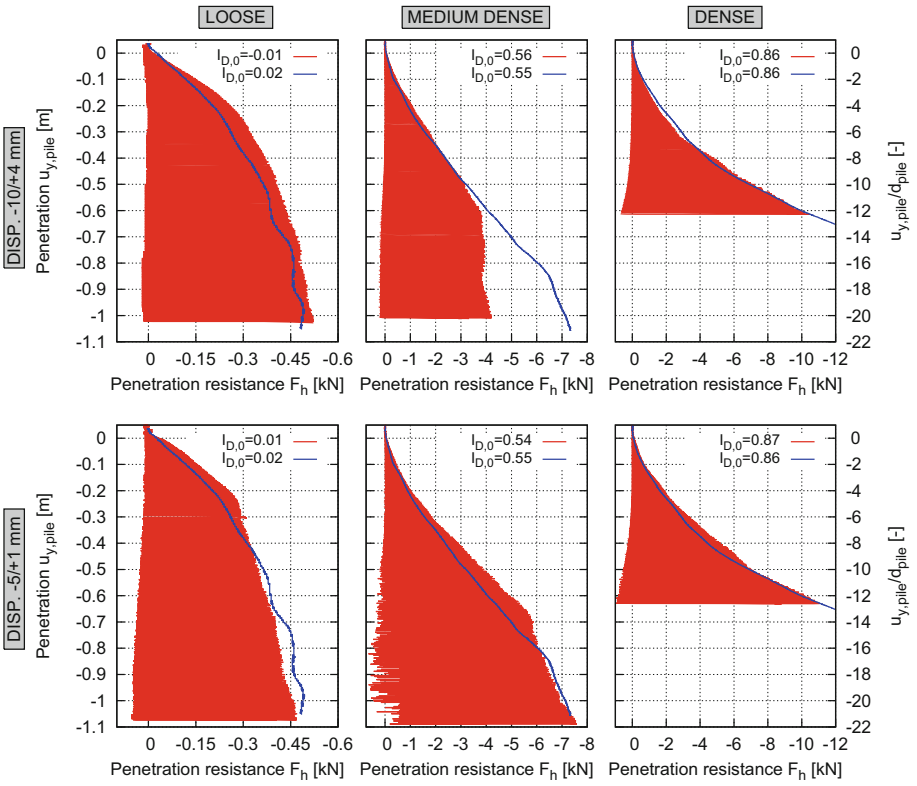

Fig. 6. Comparison of the evolution of global penetration resistance. Large amplitude driving in the upper row and small amplitude driving in the lower row. The columns represent different initial densities from loose to dense.

the pile. Regardless the amplitude, for medium dense and dense sand, above depths of about 0.6 m, the limit value during cyclic penetration is almost equal to the monotonic resistance. In medium dense sand, large penetration depths and amplitudes lead to a significantly lower maximum penetration resistance. In 1 m depth, only about 60% of the monotonic resistance are reached. Whether a similar effect occurs in dense sand remains unclear due to the limitation of penetration depth.

3.2 Evolution of Tip Resistance

The evolution of tip resistance with depth is depicted in Fig. 7. The figure is equally composed as Fig. 6.

In Fig. 7 it can be seen, that generally, the tip force vanishes during upward motion of the pile. The tip force during penetration is similar to the global penetration resistance, indicating that tip resistance is predominant compared to shaft resistance. Globally, similar observations like from Fig. 6 can be drawn.

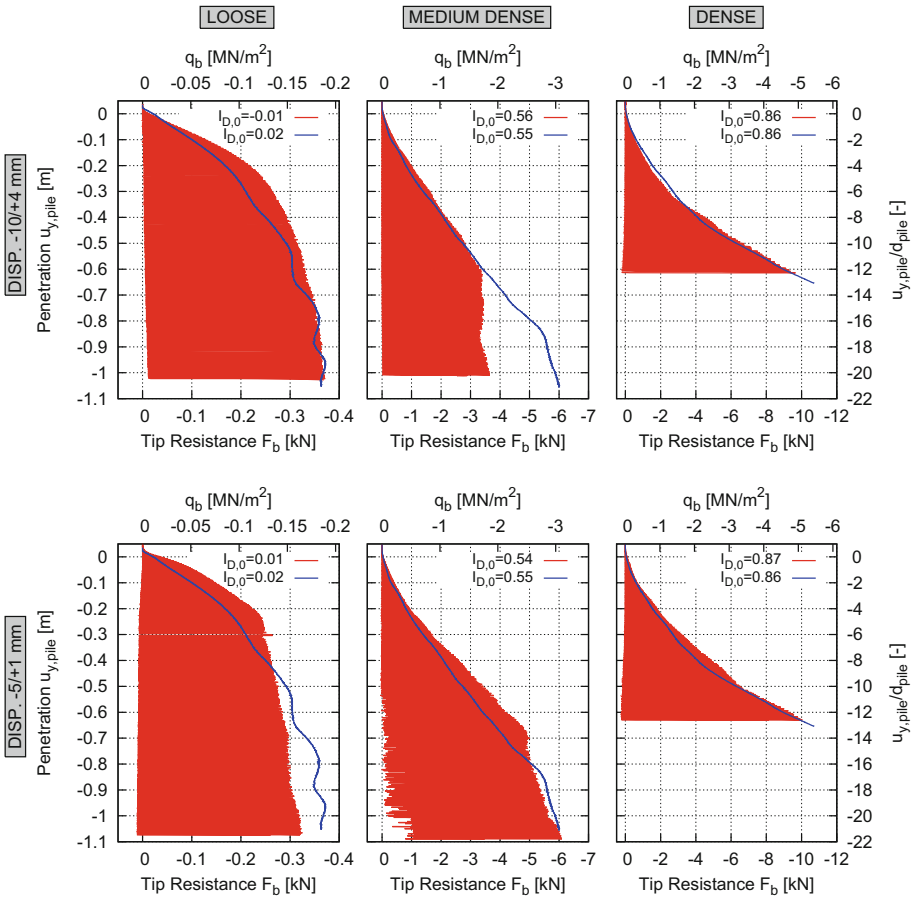

Fig. 7. Comparison of the evolution of tip resistance. Large amplitude driving in the upper row and small amplitude driving in the lower row. The columns represent different initial densities from loose to dense.

The most interesting observation in Fig. 7 is the significant difference between the cyclic tests in medium dense sand. In the case of the larger amplitude, the tip force vanishes during every upward motion of the pile and below 0.6 m the maximum tip resistance development is significantly below the monotonic tip resistance. Contrarily, for smaller upward motion and large penetration depths, the tip force decreases during upward motion, but remains compressive. Furthermore, the maximum tip force developed during penetration is very similar to the monotonic curve. A certain displacement amplitude resulting in a clear stress relief below the pile tip seems to be necessary to facilitate the penetration compared to jacking. For shallow penetration the monotonic resistance is always reached even though the tip force vanishes during upward pile motion. These

observations are in accordance with the in-situ results of Cudmani [4] for small penetration depths.

3.3 Evolution of Shaft Resistance

Similarly to the preceding figures, Fig. 8 shows the evolution of shaft force with penetration depth.

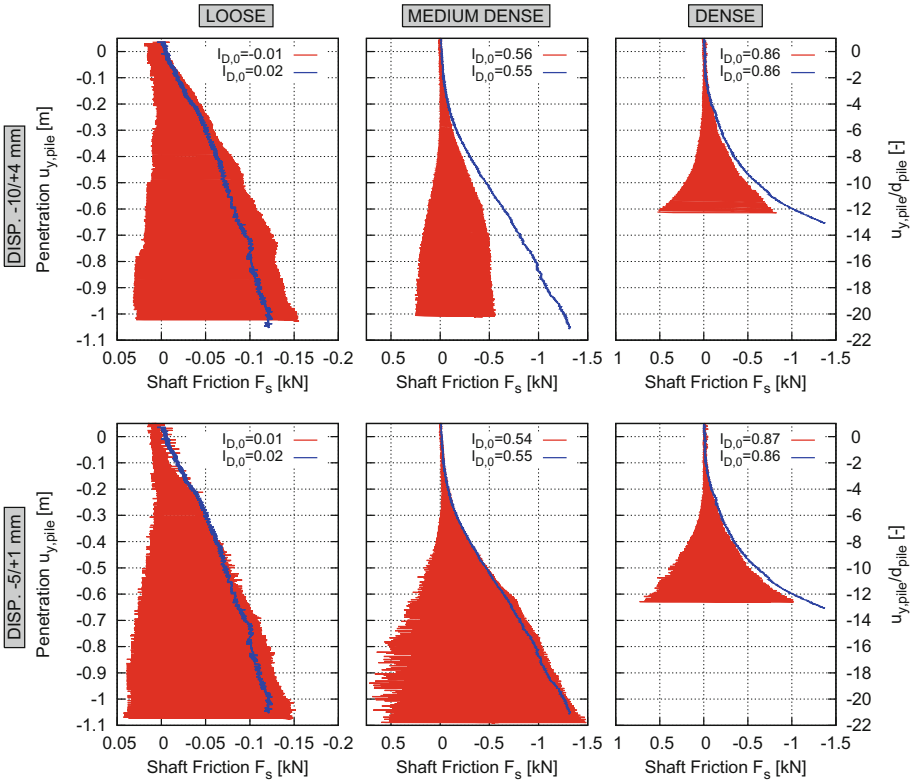

Fig. 8. Comparison of the evolution of shaft resistance. Large amplitude driving in the upper row and small amplitude driving in the lower row. The columns represent different initial densities from loose to dense.

In all tests, more shaft friction is mobilized during penetration compared to the pullout phase. This leads to a more or less pronounced asymmetry of both envelope curves. It is interesting to notice that the shaft friction during upward motion in loose sand is almost negligible indicating very low radial stresses acting on the pile. In these tests, the maximum shaft friction is slightly higher compared to monotonic penetration. A stronger densification due to cyclic penetration can be considered as the cause for this increase of shaft capacity. The tests in medium

dense sand clearly reveal the occurrence of the so-called friction fatigue effect in the case of large amplitude cycling. Throughout the whole test, the maximum shaft friction during penetration is clearly below the monotonic curve. Contrarily, for small amplitudes, the developed maximum resistance almost perfectly corresponds to the monotonic resistance. Even though the amount of upward motion is smaller, more friction is mobilized in the pullout phases compared to the test with large amplitude. This indicates, that the global stress regime acting on the pile is higher for small amplitude cycling and friction fatigue does not occur. In dense sand, friction fatigue does not play a major role although slightly lower shaft friction is observed for large amplitude cycling.

Large amplitudes in combination with medium dense soil conditions seem to be beneficial for the occurrence of friction fatigue [20]. The reason why friction fatigue is not so pronounced in the other tests may be due to the inability of loose sand for arching and the lack of dense sand for significant contraction.

3.4 Cyclic Evolution of Tip Resistance

Figure 9 investigates the cyclic evolution of tip resistance in detail. Therefore, a short section in about 0.5 m penetration depth is depicted.

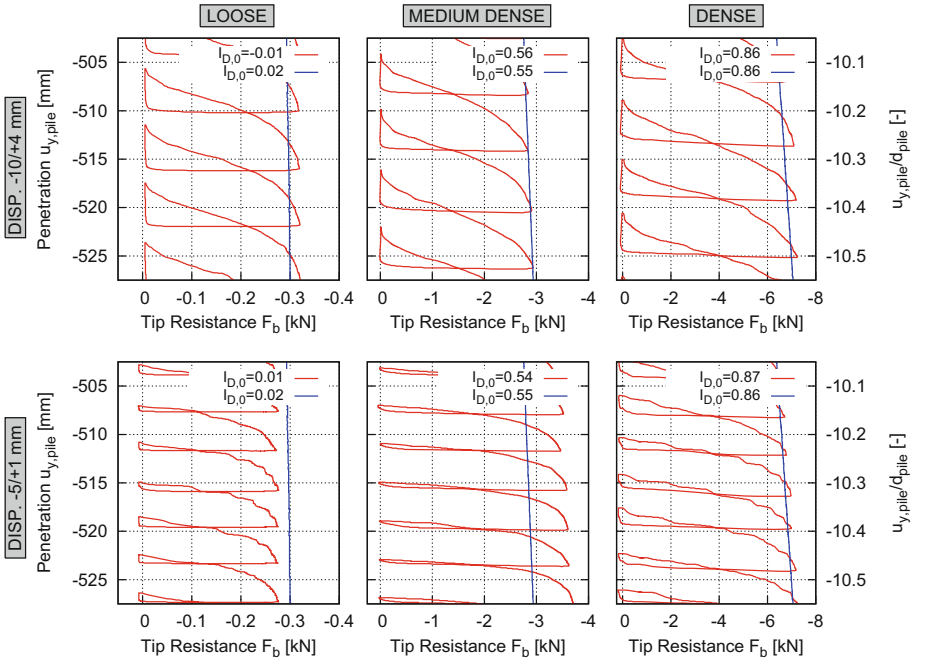

Fig. 9. Comparison of the cyclic evolution of shaft resistance in 0.5 m depth. Large amplitude driving in the upper row and small amplitude driving in the lower row. The columns represent different initial densities from loose to dense.

As it was shown before, the maximum tip force increases with soil density. However, apart from the magnitude of developed force, the evolution of tip resistance is qualitatively similar for all three densities. Its shape depends mainly on the imposed pile motion. Large amplitudes lead to a S-shaped mobilization of tip resistance during the penetration phases. The tip force vanishes after about 0.3 mm of upward pile motion and remains approximately zero throughout the whole pullout phase. In the subsequent penetration phase, the initial stiffness is very low, leading to slow increase of tip resistance. However, a section with zero tip force during penetration as described by Cudmani [4] for vibratory tests is not apparent, see also Sect. 4. This indicates that the pile tip does not lose contact to the sand. Although the tip force also vanishes in the tests with smaller upward motion of the pile, a considerably higher reloading stiffness is observed. Unloading and reloading stiffness are very similar. The tip resistance appears to reach a limit state that lies in the range of the monotonic resistance. In the cyclic test with small amplitude in medium dense sand, the maximum tip resistance exceeds the monotonic test, however, the amount can be explained with local differences of void ratio [19].

Figure 10 shows detailed cycles in a depth of about 1 m for the tests in loose and medium dense sand. The tests in dense sand have not reached this depth and are therefore not shown.

In loose sand, the evolution of tip resistance is similar in 1 m and 0.5 m depth. However, for the tests in medium dense sand, significant differences can be identified. Although the qualitative behavior is comparable to Fig. 9, the maximum tip resistance during penetration with large amplitude is substantially lower compared to the other cyclic test and to the monotonic penetration resistance.

As will be shown in Sect. 4, the observed cyclic patterns of the evolution of tip resistance have marked parallels to the tip resistance measured during vibro-penetration [4]. The measurements obtained with large amplitudes show the characteristics of the so-called cavitational penetration mode while the tests with smaller amplitudes have more similarities with the so-called non-cavitational mode [4]. A combination of large upward displacement and little penetration per cycle seems to be a trigger for the cavitational penetration mode. The non-cavitational mode occurs for small upward displacements and large effective penetration.

3.5 Cyclic Evolution of Shaft Resistance

Figure 11 shows the cyclic evolution of shaft force for the same section as Fig. 9 in a penetration depth of about 0.5 m.

The evolutions of shaft friction in the tests with large amplitudes exhibit an alternation between significant resistance in the penetration phases and very low or slightly positive resistance in the pullout phases. An increase of shaft friction during the first $4 \div 6$ mm of penetration is observed. There seems to occur a strong increase of radial stress acting on the pile in this phase. A limit shaft resistance is reached only in loose and medium dense sand. After the reversal of pile motion, the shaft friction is very low and is only slowly mobilized during

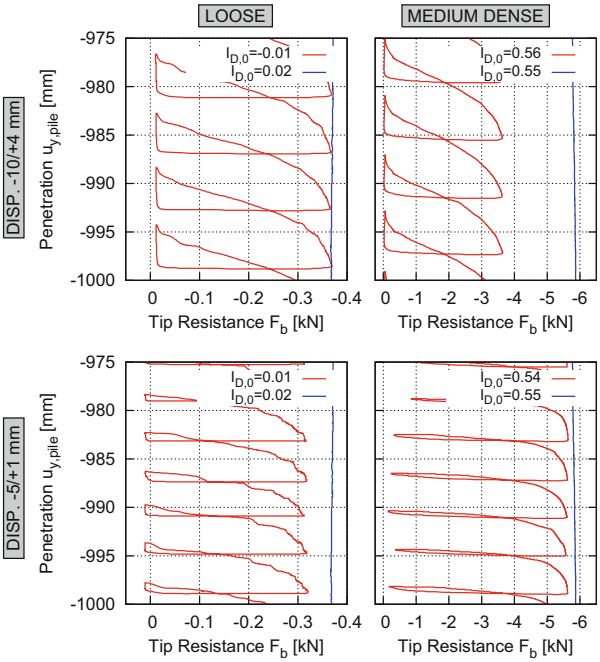

Fig. 10. Comparison of the cyclic evolution of tip resistance in 1 m depth. Large amplitude driving in the upper row and small amplitude driving in the lower row. The columns represent different initial densities from loose to medium dense.

the pullout phase. In the case of loose and medium dense sand, the shaft friction remains very small throughout the whole phase indicating very low stresses acting on the pile.

The penetration phase is qualitatively similar in the tests with smaller amplitude, but the occurring shaft resistance is larger. It is almost equal to the monotonic resistance in medium dense and dense sand. The increase of shaft friction is stronger during the first phase of penetration, thus, the shear stiffness of the soil around the pile is higher compared to the tests with smaller amplitude. The pullout phases reveal more differences between the tests with different amplitudes. Even though the amount of upward motion is lower in the small amplitude tests, more friction is mobilized during the pullout phase. This indicates that the stress relief that was observed in the test with large amplitude does not take place. The stress regime seems to change less during small amplitude cycling and a limit state is not reached in the pullout phase. This observation supports the conclusions by White and Lehane [20] made on the basis of cyclic interface tests with and without shear stress reversal. They found out that friction fatigue is significantly more pronounced in the case of two-way cycling (with shear stress reversal). In the light of these findings, it can

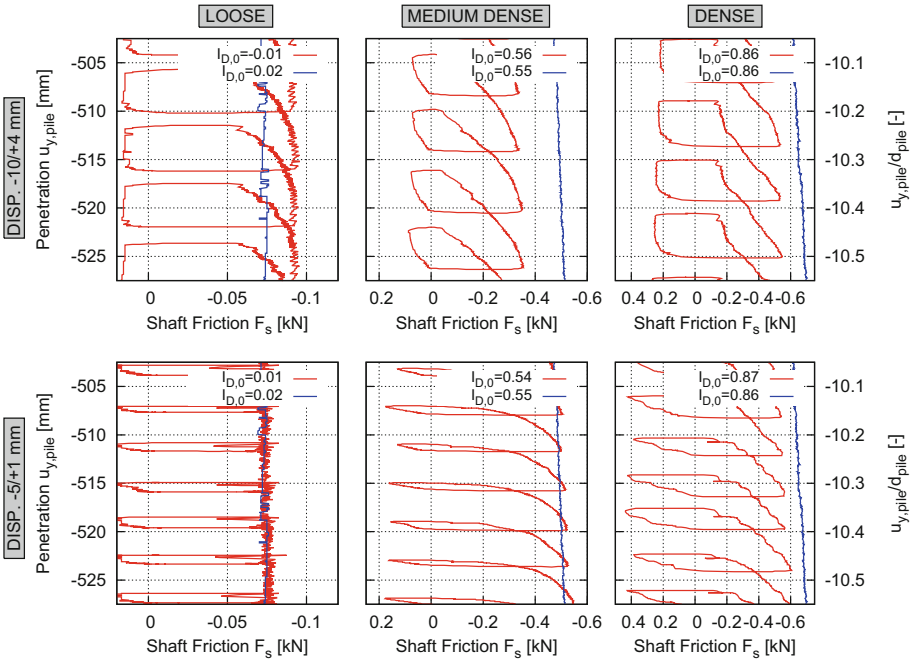

Fig. 11. Comparison of the cyclic evolution of shaft resistance in 0.5 m depth. Large amplitude driving in the upper row and small amplitude driving in the lower row. The columns represent different initial densities from loose to medium dense.

be assumed that the shear stress does not reverse clearly along the whole pile shaft in the small amplitude pile penetration tests presented here.

4 Comparison with Vibratory Tests

The comparison with existing measurements during vibro-driving processes is used in this section to validate the presented model tests with regard to real pile driving and to demonstrate the parallels between cyclic and vibro-driven penetration.

Figure 12 shows some measurements from Cudmani and Huber [4,10] obtained in two types of test series: Fig. 12(a) and (b) during in field tests on a test site near Karlsruhe, Germany and Fig. 12(c) and (d) in calibration chamber tests (CC) using a dry sand that is very comparable to the one used in the present study. The results are displayed in the form chosen for the figures in this paper. Three representative cycles are shown, whereby the second cycle is highlighted. Vertical displacement downwards is negative and the measured tip force is expressed in terms of tip resistance q_b. The pile in the field tests had a length of about 7 m and a diameter of 0.16 m. The pile tip was conical with an opening angle of about 100° [10]. The chosen sections are from a depth of 5 m in

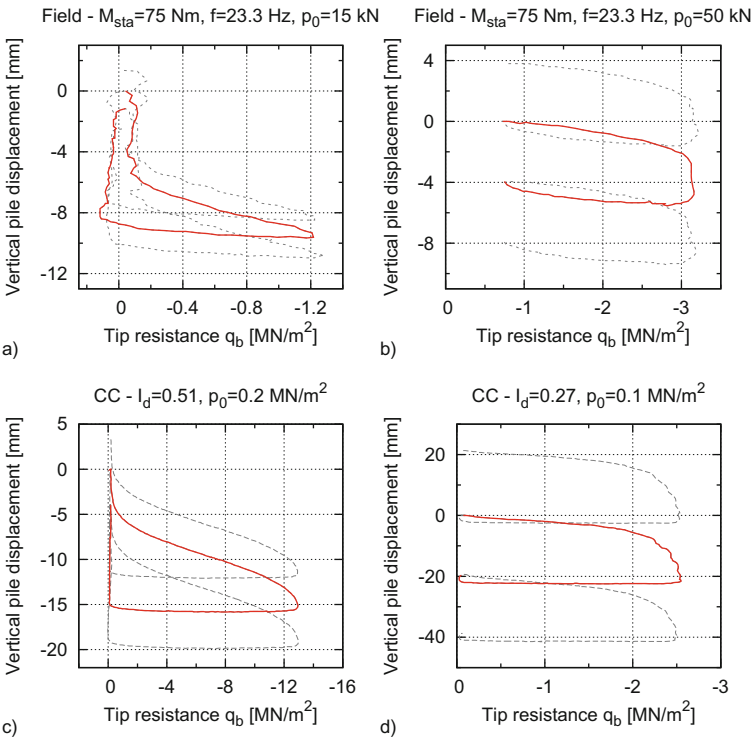

Fig. 12. Measurements during vibratory penetration: (a), (b) field tests and (c), (d) calibration chamber tests (from Cudmani [4] replotted with the sign convention of this paper)

sandy gravel below the ground water table. In Fig. 12(a) and (b) different static driving forces F_0 have been used that result in different penetration modes (the static moment M_{sta} is equal). The model pile for the CC tests was very similar to CPT equipment. The diameter of the model pile was 36 mm and the opening angle of the tip 60°. Both tests have been performed with similar parameters (static force $F_0 = 0.8\,\mathrm{kN}$, frequency $f = 32 - 35\,\mathrm{Hz}$ and coefficient of earth pressure $K = 1$). Two different penetration modes are observed here due to a variation of density and stress level p_0.

Figure 12(a) and (c) reveal the occurrence of the so-called cavitational pile driving mode whereas the results in Fig. 12(b) and (d) correspond to the non-cavitational mode. Although strong parallels are evident between field and calibration chamber measurements, also some differences can be seen. In the field test results shown in Fig. 12(a), the phase with negligible tip resistance at the beginning of each penetration phase is very pronounced compared to Fig. 12(c). Here, the mobilization of tip resistance begins earlier. This may be a consequence of the different tip angles. Considering Fig. 12(b) and (d), the most obvious difference is that the tip pressure does not vanish during the phases of upward

motion in Fig. 12(b), while it actually does in Fig. 12(d). Furthermore, the reach of a limit penetration resistance is more pronounced in Fig. 12(b).

Especially the calibration chamber test results are very similar to those of the quasistatic tests presented in this paper. They demonstrate that in quasistatic tests some important effects of vibro-penetration can be investigated. The evolution of stresses below the pile toe principally depends on the cyclic pile motion. The ratio between penetration per cycle and upward pile motion appears to be an indicator for the occurring penetration mode. Both, the results presented here as well as Cudmani's measurements [4] show that the most frequent penetration mode is the cavitational one.

These observations lead to the statement that for a first validation step for numerical models of vibratory pile driving in granular soils, also quasistatic boundary value problems can be used. Due to the prescribed pile displacement, the implementation of the test paths is very easy and a quantitative comparison can be drawn on the basis of the developed soil resistance.

5 Towards a Numerical Simulation of the Tests

This section serves to give indications towards a successful simulation of the presented test results and to demonstrate the encountered challenges.

5.1 Model Setup and Description of Soil Behavior

Pile penetration processes are usually simulated using the so-called zipper technique that was established systematically by Cudmani [4]. The pile is introduced as a rigid surface in contact with the soil. It possesses a pre-pile that represents an initial cavity in the soil. The rounded pile tip expands this cavity during penetration until the full pile diameter is reached. A similar model is described in more detail in [2] in this book. A schematic illustration of the applied FE model is shown in Fig. 13(a). More details are given in Appendix A.

The classic von Wolffersdorff hypoplasticity [21] in combination with the extension by Niemunis and Herle [13] has been shown for many times to perform well for simulations of monotonic penetration problems [4,7,19]. However, considering cyclic penetration, the model suffers from serious shortcomings. Substantial problems for the model (and most others) arise from the following characteristics:

- Large numbers of cycles
- Spatial and temporal variation of strain amplitudes
- Large changes of the stress level with stresses up to a few MN/m^2 during penetration and negligible stress during upward motion of the pile

A discussion on the shortcomings of the hypoplastic model for typical deformation paths of pile penetration is also provided in [2] in this book. Nevertheless, the model is used here to illustrate the considerable challenges for realistic simulations of cyclic penetration processes. The applied soil parameters are given in Appendix A.

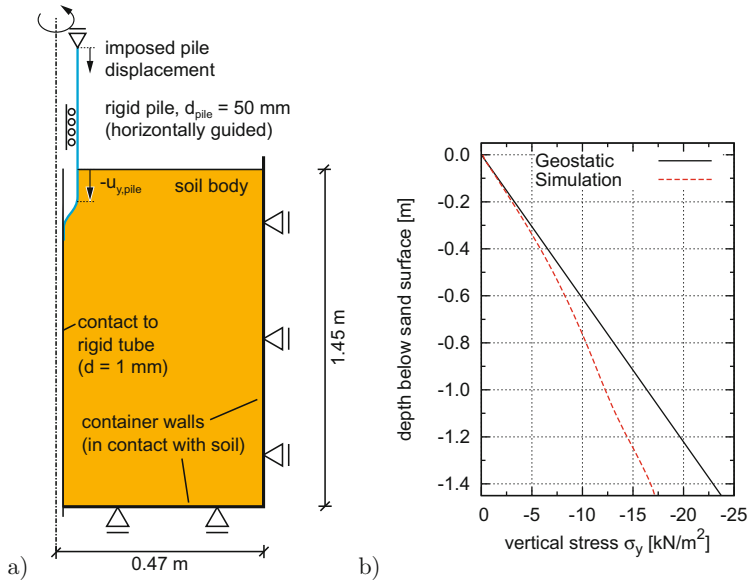

Fig. 13. (a) Schematic illustration of a suitable FE model for the simulation of the tests and (b) calculated initial stress profile in medium dense, dry sand ($I_{D,0} = 0.55$)

5.2 Initial Conditions

In test containers with rigid side walls, the initial stress field in the soil can differ from geostatic conditions due to silo effects. As shown by Vogelsang et al. [17] and Vogelsang [19], a satisfactory estimation of the initial soil stresses can be obtained by FE simulation of the soil deposition. A simple technique using a layered activation of the actual soil weight led to very realistic results. The simulation methods are described in detail in [17, 19].

Figure 13(b) investigates the soil stresses after the soil deposition for the test container used in this study. It shows the calculated stress profile in the center of a medium dense sample. From Fig. 13(b) can be seen that silo effects remain negligible up to a depth of about 0.5 m. Even in 1.1 m depth, which is the maximum depth reached in the pile penetration tests, the influences of silo effects on the initial stress distribution are moderate. With regard to a FE simulation of the subsequent pile penetration, a consideration of silo effects is therefore not of vital importance. A geostatic stress field with $K_0 = 0.4$ should be a good start for simulations of the pile tests. Once this validation step is achieved, a better back-calculation may be obtained when silo effects are considered.

5.3 Test Paths

Applying quasistatic FE formulations, each phase of downward and upward motion can be interpreted as a simulation step with the corresponding constant

displacement velocity. Using a dynamic FE code, such an implementation of the test paths would lead to velocity jumps and singularities of acceleration around the reversal points. These should therefore be smoothed, for example using the smooth step amplitude function in ABAQUS [16]. Another way is to idealize the zigzag test paths of the experiments as a sinusoidal function with a downward trend (like e.g. done in [2]). Applying explicit integration schemes, it may be necessary to shorten the simulation time compared to the physical time scale in order to minimize the computation time [8]. However, it has to be ensured the process remains mostly quasistatic in order to avoid problems arising from the reflecting boundaries.

5.4 Contact Modeling

The steel surface of the pile is rather smooth, so simple contact formulations like the Coulomb friction model should be able to capture the major effects. Based on interface shear tests [19], the friction angle between sand and steel can be estimated to $12 \div 15°$. Another important setting parameter for the contact model is the treatment of the contact behavior in normal direction (separation on/off in ABAQUS [16]). Since a sand-steel interface cannot support tensile stresses, a restriction of the contact kinematics excluding a separation of the contact surfaces is physically not justifiable. However, a separation of the contact in normal direction is not to be expected here due to the steep angle of the tip cone and its exclusion can sometimes be numerically beneficial. In the present case, the simulations turned out to run more stable without a restriction of the contact kinematics. The consequences of this input parameter are illustrated in Fig. 14. It shows a short section of the load-displacement curve for penetration with the $-10/+4$ mm displacement sequence. The deformed FE mesh in the highest point of pile motion during one cycle is shown on the right. As can be seen, a gap forms below the pile tip. In the load curve, the phase without contact below the pile tip can also be recognized during upward and in the first part of the downward

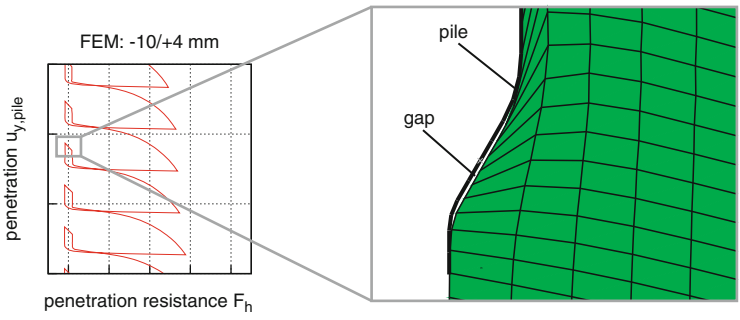

Fig. 14. Load-displacement curve during cyclic penetration and mesh configuration in the highest point of the pile during one cycle

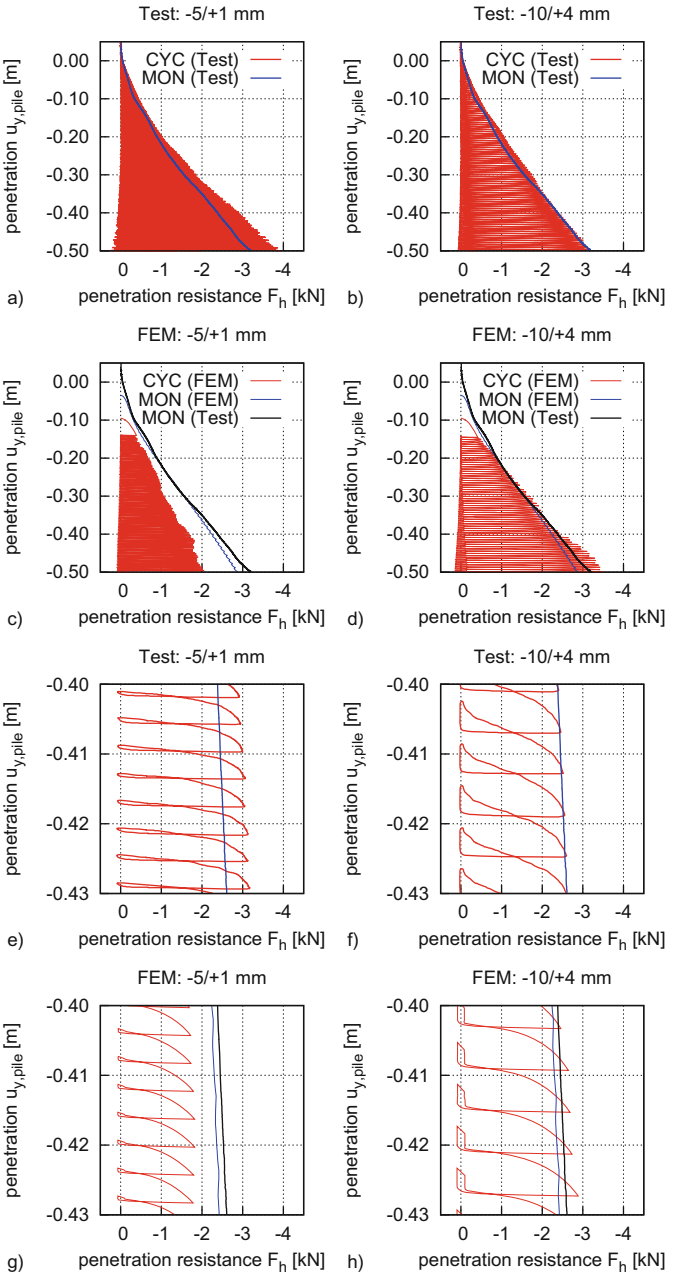

Fig. 15. Comparison of experimental and numerical results of cyclic penetration resistance in medium dense sand: (a)–(d) overview of the first 0.5 m and (e)–(h) detail of cycles in 0.4 m depth. Small amplitude driving in the left column and large amplitude driving in the right column. (ABAQUS/STANDARD with geostatic initial state)

motion. Such phases have not been identified in the experiments and have to be considered as numerical artefacts.

5.5 Some Simulation Results

Figure 15 presents exemplary results from back-calculations of the three model tests in medium dense sand. The simulations concentrate on the first 0.5 m of penetration. The left column corresponds to the cyclic test with small amplitude (−5/+1 mm) and the right column to the one with larger amplitude (−10/+4 mm). The first row, Fig. 15(a) and (b), gives an overview of the experimental results and the second row, Fig. 15(c) and (d), of the simulation results. Figure 15(e)–(h) show details of the cycles in about 0.4 m depth in the same order. Since silo effects are negligible within the first 0.5 m depth, a geostatic initial state was chosen to simplify the simulations.

In both cyclic experiments, the monotonic limit resistance is reached during the first 0.5 m of penetration, Fig. 15(a) and (b). Considering the numerical simulations, this behavior is observed only for the test with −10/+4 mm displacement sequence, Fig. 15(d). The smaller penetration rate (per cycle) of the test with the −5/+1 mm sequence leads to a lower penetration resistance, Fig. 15(c). The detailed presentation of selected cycles reveals that the qualitative behavior of the experiment is better modeled in the case of small upward motion of the pile (−5/+1 mm), Fig. 15(g). The loosening of the soil around the pile tip during large displacement upwards cannot be reproduced by the numerical model, Fig. 15(h). Thus, the stiffnesses during reloading do not differ significantly. As it is demonstrated in [2], these deficits are probably attributed to the performance of the soil model in the occurring deformation paths.

6 Conclusions

Monotonic and cyclic full-model pile penetration tests in dry sand have been carried out to investigate the influence of cyclic penetration on the soil resistance. The tests include some major effects of vibratory pile driving but offer advantages such as an easier systematic investigation of the process and the achievement of very suitable experimental data for model validation purposes.

During cyclic pile penetration, monotonic and cyclic effects on soil resistance are counteracting. Monotonic pile motion tends to increase the stress level around the pile, while superimposed cycling can cause a substantial stress relief. The ratio between upward motion and effective penetration per cycle is an indicator for the developed soil resistance compared to the monotonic resistance. Large ratios lead to a facilitated penetration, whereas by working with low ratios similar stresses than during monotonic penetration are observed. The beneficial effect of cyclic penetration regarding the driveability is most pronounced in medium dense sand in combination with large pile displacement amplitudes.

The observed stress paths during penetration with large amplitude are very similar to the cavitational vibratory penetration mode. Cyclic penetration with

lower amplitude corresponds to the non-cavitational vibratory mode. Friction fatigue along the shaft becomes evident in medium dense sand when large cycles are imposed.

The suitability of commonly used simulation methods [4,7,8] is questionable for cyclic penetration processes, mainly due to deficiencies of most soil models to perform in typical deformation paths. However, the applied FE model with hypoplastic description of the soil behavior is qualitatively capable to reproduce important effects observed in the experiments. The improvement of available soil models is a primary task in order to obtain more realistic simulations of pile penetration processes.

A Details of the FE Model

Details concerning the setup of the numerical model can also be found in [19]. Axisymmetric CAX4 elements are used. The horizontal length of the elements near the symmetry axis is greater than the height in order to reduce mesh distortion problems. An impression of the FE mesh near the pile tip can be received in Fig. 14. In order to ensure a better numerical stability, the first 0.05 m of soil are replaced by a uniformly distributed pressure equivalent to the soil weight. The initial conditions are assumed to be geostatic with $K_0 = 0.37$. The initial void ratio is chosen according to the corresponding experiment (Table 1). The pile penetration begins in 0.1 m depth (position of the pile shoulder with respect to the sand surface). After an initial phase of 30 mm monotonic displacement the cyclic pile motion is prescribed. The increment size corresponds to a pile displacement of about 0.06 mm.

The material parameters used for the simulations are given in Table 2. Note that these differ from the parameters used in [2]. The calibration procedure is described by Vogelsang [19]. The slight differences of the current test sand compared to older charges (see Sect. 2.3) have not been considered during the calibration.

The Coulomb friction model is used to model the interaction between soil and pile resp. soil and side walls. A friction angle of 12° is chosen for the pile-soil and 22° ($\approx 2/3\varphi_c$) for the soil-wall interface.

Table 2. (a) Applied constitutive parameters of the test sand and (b) additional constitutive parameters of the extended hypoplastic model with intergranular strain

a)

φ_c[°]	h_s [MPa]	e_{c0}	e_{d0}	e_{i0}	α	β	n
33.1	19000	0.865	0.549	1.0	0.1	1.25	0.285

b)

R	m_R	m_T	β_r	χ
5×10^{-5}	2.5	1.25	0.1	4.0

References

1. ASTM Standard D4254-91: Standard test method for minimum index density and unit weight of soils and calculation of relative density. Annual Book of ASTM Standards. ASTM International, West Conshohocken (2006)
2. Chrisopoulos, S., Vogelsang, J., Triantafyllidis, T.: FE simulation of model tests on vibratory pile driving in saturated sand. In: Triantafyllidis, T. (ed.) Holistic Simulation of Geotechnical Installation Processes. LNACM, vol. 82, pp. 124–149. Springer, Cham (2017)
3. Choi, S.-K., Lee, M.-J., Choo, H., Tumay, M.T., Lee, W.: Preparation of a large size granular specimen using a rainer system with a porous plate. Geotech. Test. J. **33**(1), 45–54 (2009)
4. Cudmani, R.O.: Statische, alternierende und dynamische Penetration in nichtbindigen Böden. Dissertation, vol. 152. Publications of the Institute of Soil Mechanics and Rock Mechanics, University of Karlsruhe (2001)
5. Dierssen, G.: Ein bodenmechanisches Modell des Vibrationsrammens in körnigen Böden. Dissertation, vol. 133. Publications of the Institute of Soil Mechanics and Rock Mechanics, University of Karlsruhe (1994)
6. DIN 18126: Bestimmung der Dichte nichtbindiger Böden bei lockerster und dichtester Lagerung. Beuth-Verlag (1996-11)
7. Grabe, J., König, F.: Zur aushubbedingten Reduktion des Drucksondierwiderstands. Bautechnik **81**(7), 569–577 (2004)
8. Henke, S.: Untersuchungen zur Pfropfenbildung infolge der Installation offener Profile in granularen Böden. Habilitation, vol. 29. Publications of the Institute of Geotechnical Engineering and Construction Management, TU Hamburg-Harburg (2013)
9. Hereema, E.P.: Predicting pile driveability: heather as an illustration of the "friction fatigue" theory. In: SPE European Petroleum Conference, London (1978)
10. Huber, G.: Vibrationsrammen: Großmaßstäbliche Versuche. In: Workshop "Vibrationsrammen", Karlsruhe, Germany, pp. 13–30 (1997)
11. Lehane, B.M., White, D.J.: Lateral stress changes and shaft friction for model displacement piles in sand. Can. Geotech. J. **42**, 1039–1052 (2005)
12. Linder, W.-R.: Zum Eindring- und Tragverhalten von Pfählen in Sand. Dissertation, Fachbereich für Bauingenieur- und Vermessungswesen, TU Berlin (1977)
13. Niemunis, A., Herle, I.: Hypoplastic model for cohesionless soils with elastic strain range. Mech. Cohesive Frictional Mater. **2**(4), 279–299 (1997)
14. Rimoy, S.P.: Ageing and axial cyclic loading studies of displacement piles in sand. Dissertation, Department of Civil and Environmental Engineering, Imperial College London (2013)
15. Rodger, A.A., Littlejohn, G.S.: A study of vibratory driving in granular soils. Géotechnique **30**(3), 269–293 (1980)
16. Simulia: Abaqus Users Manual. Version 6.14 (2014)
17. Vogelsang, J., Zachert, H., Huber, G., Triantafyllidis, T.: Effects of soil deposition on the initial stress state in model tests: experimental results and FE simulation. In: Triantafyllidis, T. (ed.) Holistic Simulation of Geotechnical Installation Processes. LNACM, vol. 77, pp. 1–20. Springer, Heidelberg (2015). doi:10.1007/978-3-319-18170-7_1
18. Vogelsang, J., Huber, G., Triantafyllidis, T., Bender, T.: Interpretation of vibratory pile penetration based on digital image correlation. In: Triantafyllidis, T. (ed.) Holistic Simulation of Geotechnical Installation Processes. LNACM, vol. 80, pp. 31–51. Springer, Heidelberg (2016). doi:10.1007/978-3-319-23159-4_2

19. Vogelsang, J.: Untersuchungen zu den Mechanismen der Pfahlrammung. Dissertation, Publications of the Institute of Soil Mechanics and Rock Mechanics, Karlsruhe Institute of Technology, submitted (2017)
20. White, D.J., Lehane, B.M.: Friction fatigue on displacement piles in sand. Géotechnique **54**(10), 645–658 (2004)
21. von Wolffersdorff, P.-A.: A hypoplastic relation for granular materials with a predefined limit state surface. Mech. Cohesive Frictional Mater. **1**, 251–271 (1996)

Springer

http://www.springer.com/978-3-319-52589-1

Holistic Simulation of Geotechnical Installation Processes
Theoretical Results and Applications
Triantafyllidis, T. (Ed.)
2017, VIII, 363 p. 201 illus., Hardcover
ISBN: 978-3-319-52589-1